Articles

Porous Gelatin Hydrogels: 1. Cryogenic Formation and Structure Analysis

Sandra Van Vlierberghe,[†] Veerle Cnudde,[‡] Peter Dubruel,[†] Bert Masschaele,[§] An Cosijns,[||] Ilse De Paepe,[†] Patric J. S. Jacobs,[‡] Luc Van Hoorebeke,[§] Jean Paul Remon,[||] and Etienne Schacht*[,†]

Polymer Chemistry and Biomaterials Research Group, Ghent University, Krijgslaan 281, Building S4 Bis, B-9000 Ghent, Belgium, Department of Geology and Soil Science, Ghent University, Krijgslaan 281, Building S8, B-9000 Ghent, Belgium, Department of Subatomic and Radiation Physics, Ghent University, Proeftuinstraat 86, B-9000 Ghent, Belgium, and Laboratory of Pharmaceutical Technology, Ghent University, Harelbekestraat 72, B-9000 Ghent, Belgium

Received July 14, 2006; Revised Manuscript Received September 12, 2006

In the present work, porous gelatin scaffolds were prepared by cryogenic treatment of a chemically cross-linked gelatin hydrogel, followed by removal of the ice crystals formed through lyophilization. This technique often leads to porous gels with a less porous skin. A simple method has been developed to solve this problem. The present study demonstrates that the hydrogel pore size decreased with an increasing gelatin concentration and with an increasing cooling rate of the gelatin hydrogel. Variation of the cryogenic parameters applied also enabled us to develop scaffolds with different pore morphologies (spherical versus transversal channel-like pores). In our opinion, this is the first paper in which temperature gradients during controlled cryogenic treatment were applied to induce a pore size gradient in gelatin hydrogels. With a newly designed cryo-unit, temperature gradients of 10 and 30 °C were implemented during the freezing step, resulting in scaffolds with average pore diameters of, respectively, ±116 and ±330 μm. In both cases, the porosity and pore size decreased gradually through the scaffolds. Pore size and structure analysis of the matrices was accomplished through a combination of microcomputed tomography using different software packages (μCTanalySIS and Octopus), scanning electron microscopy analysis, and helium pycnometry.

1. Introduction

The domain of tissue engineering has been studied extensively over the past decades, since there is a need for new, innovating technologies making the replacement or repair of failing tissues possible.[1,2] A frequently applied approach is the development of porous scaffolds containing bioactive compounds such as glycosaminoglycans and/or growth factors.[3−6] Autologous or allogenic cells can be seeded and cultured on these materials resulting in newly formed tissue in vitro[7] or in vivo.[7,8] In the past, a large number of materials, synthetic as well as natural, have been proposed as cell carriers. The most frequently used synthetic polymers include poly(glycolic acid), poly(D,L-lactic acid), and poly(D,L-lactic-*co*-glycolic acid) copolymers.[9−11] Common natural cell matrices include chitosan,[12,13] collagen,[14,15] and gelatin.[16−18] In the present work gelatin was selected, since it is a self-assembling, nontoxic, biodegradable, inexpensive, and nonimmunogenic material.[18] It has been widely applied in medicine as a wound dressing[19] and as an adhesive and absorbent pad for surgical use. Moreover, in previous studies on gelatin-based sponges, it was shown that acellular sponges containing gelatin have potential applications in the field of tissue engineering.[8] The gel−sol transition temperature of gelatin is approximately 30 °C. In the present work, gelatin was derivatized with methacrylamide side chains enabling chemical cross-linking to avoid dissolution at body temperature (37 °C).[20]

A material to be applied as a scaffold should fulfill certain requirements. First, high porosity is required to support diffusion of oxygen and nutrients toward the cells and drainage of waste products from the matrix. In addition, pore interconnectivity is important to promote phenomena such as cell migration and angiogenesis. Second, the porous biomaterials should be biocompatible and in some cases also biodegradable.[16,21]

The pore size required for cell ingrowth depends on the cell type seeded on the matrix.[11] For porous silicon nitride scaffolds, endothelial cells bind preferentially to scaffolds with pores smaller than 80 μm, while fibroblasts preferentially bind to larger pores (>90 μm).[14] A pore size gradient through the scaffold could be favorable in some cases.

At present, different techniques exist to fabricate porous scaffolds including porogen leaching,[9,16] phase separation,[22] emulsion freeze-drying,[11] solvent evaporation,[23] gas foaming,[24] and fiber bonding.[25]

In the present study, a combination of phase separation and freeze-drying was used to induce pore formation within gelatin hydrogels. When an aqueous gelatin solution is solidified (i.e.,

* Author to whom correspondence should be addressed. Phone: 00329264-4497. Fax: 003292644972. E-mail: Etienne.Schacht@UGent.be.
[†] Polymer Chemistry and Biomaterials Research Group.
[‡] Department of Geology and Soil Science.
[§] Department of Subatomic and Radiation Physics.
[||] Laboratory of Pharmaceutical Technology.

10.1021/bm060684o CCC: $37.00
Published on Web 01/05/2007

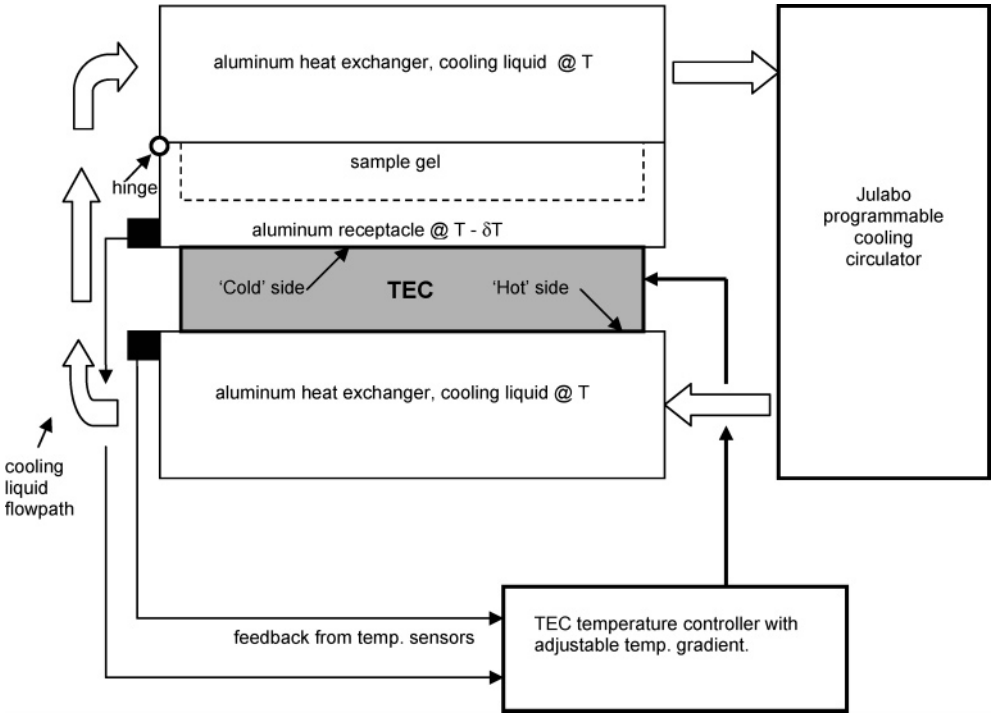

Figure 1. Schematic overview of the programmable cryo-unit applied for the preparation of the porous gelatin scaffolds.

frozen), phase separation occurs between the growing ice crystals and the concentrated gelatin solution (nonfrozen liquid microphase).[26,27] After sublimation of the ice crystals (freeze-drying), a porous scaffold originates. With a novel cryo-setup, developed in our laboratory, the cooling rate, the temperature gradient, and the final freezing temperature during the cryogenic treatment can be varied in a controlled manner. In addition, we also varied the gelatin concentration.

Scanning electron microscopy (SEM), helium pycnometry (He pycnometry), and microcomputed tomography (μ-CT) analysis were applied for evaluating the porous gelatin hydrogels developed.

2. Materials and Methods

2.1. Materials. Gelatin (type B), isolated from bovine skin by an alkaline process, was kindly supplied by Rousselot, Ghent, Belgium. Gelatin samples with an approximate isoelectric point of 5 and a Bloom strength of 257 were used. Methacrylic anhydride (MAA) was purchased from Aldrich (Bornem, Belgium) and was used as received. Dialysis membranes Spectra/Por 4 (molecular weight cutoff of 12 000−14 000 Da) were obtained from Polylab (Antwerp, Belgium). 1-[4-(2-Hydroxyethoxy)-phenyl]-2-hydroxy-2-methyl-1-propane-1-one (Irgacure 2959) was a kind gift from Ciba Speciality Chemicals N.V. (Groot-Bijgaarden, Belgium). An long wavelength UV lamp model VL-400L (Vilber Lourmat, Marne La Vallée, France) was used for sample curing.

2.2. Preparation of Cross-Linked Gelatin Hydrogels. Gelatin was chemically modified with methacrylamide side groups, as described in a previous paper.[20] A derivative with a degree of substitution of 60% was selected for this work. The degree of substitution is defined as the percentage of the free amino groups being modified. As an example, the synthesis of 10% (w/v) gelatin is given. In a typical experiment 1 g of modified gelatin was dissolved in 10 mL of distilled water at 40 °C, containing 2 mol % photoinitiator Irgacure 2959 as calculated relative to the methacrylamide side chains. The solution was then injected into the mold of the cryo-unit schematically shown in Figure 1, after which the solution was allowed to gel for 1 h at room temperature. In a final curing step, the hydrogel was exposed to UV light (276 nm, 10 mW/cm^2) for 2 h.

2.3. Preparation of Gelatin Scaffolds with Different Pore Sizes. After the chemically cross-linked hydrogel was placed in the cryo-unit, the temperature of freezing and the cooling rate were programmed with a Julabo, type FP40-ME. Under the bottom of the mold, a Peltier element (also known as a thermoelectric cooler (TEC)) was positioned. This device enables a temperature gradient of a maximum of 30 °C to be established between the top and the bottom of the mold. The TEC used was a DuraTec DT12 type from Marlow industries. The aluminum heat exchangers and the electronic TEC controller were designed, built, and assembled by the technical workshop (CWFW) of the Faculty of Sciences, Ghent University. For the samples obtained by applying a temperature gradient, the temperature at the top of the mold was the highest.

After incubation of the sample for 1 h at the final freezing temperature, the frozen hydrogel was transferred to a freeze-dryer to remove the ice crystals, resulting in a porous scaffold.

2.4. Preparation of Gelatin Scaffolds with a Dissolvable Skin. Gelatin scaffolds with a dissolvable skin were prepared as described in section 2.3. Before application of the cryogenic treatment, a 10% (w/v) solution of nonmodified gelatin was injected on the top and the bottom of the chemically cross-linked hydrogel, which was positioned in the mold of the cryo-unit. The resulting layer was 0.5 mm in thickness on a 5-mm-thick hydrogel. After cryogenic treatment and freeze-drying of the hydrogels, the samples were incubated in deionized water at 40 °C for 5 h. Freeze sections of the incubated scaffolds were made with a microtome and studied using optical microscopy (section 2.5.4).

2.5. Characterization of Porous Scaffolds. *2.5.1. Microcomputed Tomography.* In this study, a "Skyscan 1072" X-ray microtomograph was used. This compact desktop system, consisting of an X-ray shadow microscopic system and a computer with tomographic reconstruction software, generates high-resolution images for small samples (7 mm in diameter). During a measurement, both the X-ray source and the detector are fixed while the sample rotates around a stable vertical axis. Samples were scanned at a voltage of 130 kV and a current of 76 μA. Random movement and multiple-frame averaging were used to minimize the Poisson noise in the images. The spot size of the Hamamatsu microfocus tube limits the spatial resolution of the reconstructed slices to 10 μm in the *X*, *Y*, and *Z* directions. During acquisition, X-ray radiographs are recorded at different angles during stepwise rotation between 0° and 180° around the vertical axis. The

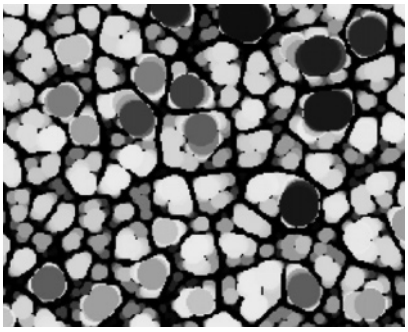

Figure 2. Principle of the pore analysis performed by μCTanalySIS.

attenuation of the X-rays passing through a sample when scanning is performed depends on the atomic number of the material and its density. These two features are crucial in the resulting contrast of the images.

After reconstruction of the two-dimensional (2D) cross-sections, three-dimensional (3D) software μCTanalySIS[28,29] was used to segment the images and determine their 3D porosity and pore size distribution. For the determination of the pore size distribution, each pore was filled with the largest sphere possible (the so-called "maximum opening"). The total volume filled by this maximum sphere was determined during the analysis. Subsequently, the software filled the total volume of each pore with a smaller sphere, while its total filling volume was determined. This process continued until the total volume of each pore was comprised with the smallest inscribed sphere, with a size of one voxel (Figure 2). From this analysis, data for all pores were acquired.

Another software program, Octopus,[30,31] was also used to analyze certain images and to show the similarity with micrographs generated using SEM. Octopus is a server/client tomography reconstruction package for parallel and cone beam geometry.

2.5.2. Scanning Electron Microscopy. The morphology of gold-sputtered scaffolds was examined using the scanning electron micrographs obtained on a Fei Quanta 200F (field emission gun) scanning electron microscope. Ten pore diameters were measured randomly, and the average pore diameter and deviation were calculated.

2.5.3. Helium Pycnometry. The porosity of the hydrogels was studied using a He pycnometer (Accupyc 1330, Norcross, GA). Each measurement was performed in duplicate.

2.5.4. Optical Microscopy. Visualization of the freeze sections obtained (section 2.4) was performed using an Axiotech 100 reflected light microscope (Carl Zeiss), with a reflected light brightfield for Köhler illumination.

3. Results and Discussion

In the present study, porous gelatin scaffolds were generated by a cryogenic treatment of a chemically cross-linked gelatin hydrogel. This leads to phase separation between the nonfrozen liquid microphase (concentrated gelatin solution) and the growing ice crystals. Finally, porous structures were obtained by lyophilization. For the development of different porous hydrogels, a specially designed cryo-unit was applied. The setup, as depicted in Figure 1, enabled us to vary different parameters during the cryogenic treatment: cooling rate, temperature gradient, and final freezing temperature. In addition, also the effect of the gelatin concentration on the material properties was studied. The materials were analyzed for their pore size, pore geometry, and their overall porosity by μ-CT, He pycnometry, SEM, and optical microscopy. Both μ-CT and SEM have been widely applied previously for evaluating porous, 3D scaffolds.[9,10,32,33]

3.1. Skin Formation during Cryogenic Treatment of the Hydrogels. We noticed by optical microscopy of freeze sections (cross-sections) of cryogenically treated hydrogels that the treatment did result in the formation of hydrogels with a less porous skin with a thickness of 100−200 μm (Figure 3, left part). The latter is a problem for cell ingrowth studies. Therefore, a simple and novel technique enabling the elimination of skin formation was elaborated. The hydrogels, prepared as described above (section 2.3), were coated on the top and bottom by a 0.5-mm-thick layer of un-cross-linked gelatin. After cryogenic treatment, the un-cross-linked top and bottom layers were dissolved by incubation in water (40 °C, 5 h). Microscopic analysis clearly demonstrated that this approach allowed us to avoid the problem of skin formation (Figure 3). This procedure was then adapted as a standard treatment in the preparation of all cryogenic hydrogels described in this work.

3.2. Effect of Gelatin Concentration. As a first variable for the preparation of hydrogels, the gelatin concentration (expressed as % w/v) was varied. The conditions used for the hydrogel preparation as well as the pore analysis data obtained using μ-CT, He pycnometry, and SEM are listed in Table 1. The pore sizes of both types of hydrogels, as visualized by μ-CT and SEM analysis, are shown in Figure 4.

From the results, it can be concluded that both the porosity and the pore size decreased with an increasing amount of gelatin. There are two possible explanations for the observed findings.

First, a higher gelatin concentration could result in an increasing nucleation rate and thus in a larger number of pores. Nucleation depends on the instability of the liquid phase and on the diffusion of atoms into clusters. The former increases with decreasing temperature; the latter increases with increasing temperatures. A higher gelatin concentration resulted in a decrease of the freezing temperature of the solvent (in this case water). As a consequence, the mobility of the atoms to diffuse into clusters was higher, and the nucleation rate increased.

Second, by comparison of the 5−15% (w/v) scaffolds, the more concentrated hydrogels could possess a decreased heat and protein transfer and thus result in smaller pores. A combination of both is most likely the most plausible explanation.

The pore sizes, measured using SEM, were somewhat lower than the pore sizes obtained using μ-CT (Table 1, Figure 4). This is due to the fact that, in the case of μ-CT, pore diameters are calculated based on the amount of pixels present in the pore diameter. Thus, when taking into account the pixels of the pore wall itself, the pore size obtained will be at least 20 μm higher (since one pixel corresponded with 10 μm), depending on the pore wall thickness. A combination of different techniques, both with its advantages and disadvantages (destructive (SEM) vs nondestructive (μ-CT), objective (SEM) vs subjective (choice of thresholding parameters using μ-CT), 100 nm resolution (SEM) vs 10 μm resolution (μ-CT), 2D (SEM) versus 3D imaging (μ-CT)), is thus essential to obtain a complete material analysis.

The difference in porosity between the scaffolds was studied by He pycnometry and μ-CT analysis. The μ-CT data showed a smaller variation between the porosities of the samples compared to that shown by pycnometry measurements (Table 1). In our opinion, the porosities obtained from pycnometry experiments are more realistic. The latter technique is not limited to a resolution of 10 μm since it is based on the intrusion of helium in the porous scaffolds. In the present work, we have selected the μ-CT tresholding parameters in such a way that no scaffold material was excluded. The disadvantage of the latter approach was that some noise voxels were then considered as material, leading to a lower decrease in porosity. The higher

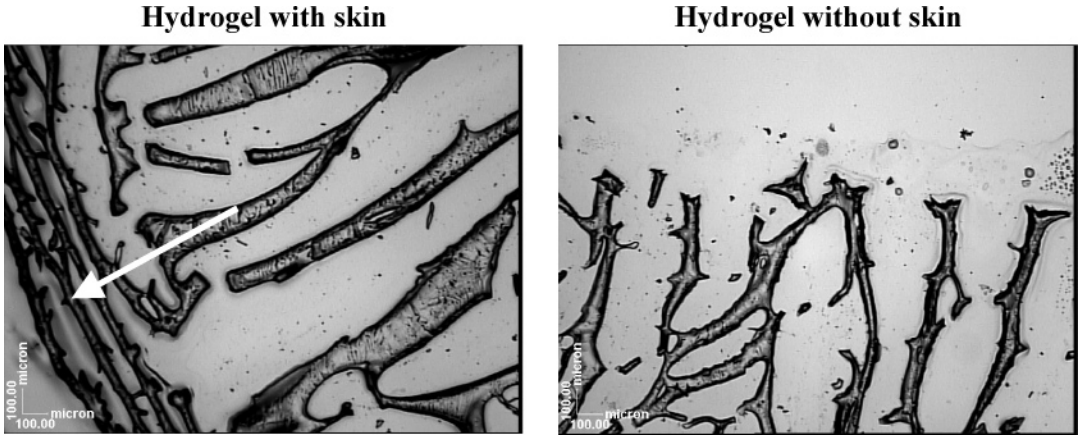

Figure 3. Optical microscopy visualization of hydrogel freeze sections obtained using a microtome. The left and right panels represent a hydrogel, respectively, with and without a nonporous skin. The skin present on the left hydrogel is indicated by the white arrow. The scale bars represent 100 μm.

Table 1. Experimental Parameters and Pore Analysis Data for Type I, II, and III Scaffolds

sample	type I	type II	type III
gelatin concentration	5% (w/v)	10% (w/v)	15% (w/v)
cooling rate	0.15 °C/min	0.15 °C/min	0.15 °C/min
final freezing temperature	−30 °C	−30 °C	−30 °C
temperature gradient	0 °C	0 °C	0 °C
porosity (μ-CT)	86 ± 0.68%	83 ± 2.63%	82 ± 1.33%
average pore diameter (μ-CT)	160 μm	135 μm	105 μm
average pore diameter (SEM)	147 ± 41 μm	117 ± 37 μm	70 ± 24 μm
porosity (pycnometry)	96 ± 0.4%	91 ± 0.7%	78 ± 0.6%

porosity of the 5% (w/v) gelatin compared to that of the 15% (w/v) gelatin is clearly illustrated in Figure 4 (first and second rows).

An important prerequisite for a scaffold to be applied as a biomaterial is the fact that the material should possess interconnecting pores. Pore interconnectivity can be studied by μ-CT. To analyze the reconstructed images, double thresholding based on the gray value histogram of the images had to be performed using μCTanalySIS.[34] After thresholding, each pore detected inside the binary images was labeled and analyzed in 3D. On the basis of the maximum opening of each pore, the binary images were then rewritten, labeling each pore with a certain gray value corresponding to a certain maximum opening size. The gray value of a pore in the 2D segmentations (Figure 4, top row) indicated the diameter of the largest inscribed sphere in the pore network concerned. Figure 4 illustrates two cross-sections after analysis with μCTanalySIS. A low contrast between the material borders and the pores, in combination with small amounts of noise, containing similar gray values to those of the material borders, led to small errors in the resulting thresholded images. Figure 4 (top left) suggested that the pores of the 5% (w/v) scaffold were interconnecting. The complete pore network was labeled in white, thus either belonging to the same pore network or belonging to different pore networks with the same maximum opening. In the 15% (w/v) gelatin (Figure 4, top right) more individual pores were detected, each belonging to a different pore network.

3.3. Effect of Cooling Rate. In addition to the gelatin concentration, the cooling rate of the gelatin solution was also varied. Literature data describe the influence of the cooling rate on the nucleation and growth of ice crystals and thus on the

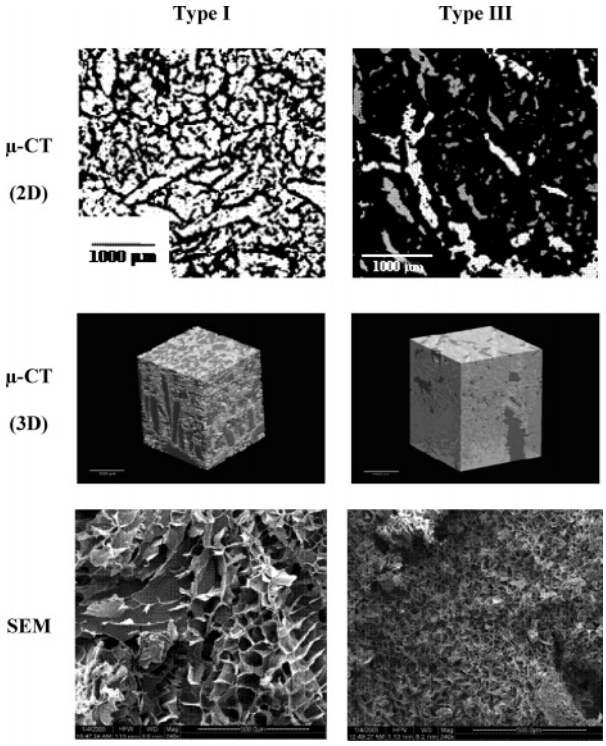

Figure 4. μ-CT (2D and 3D) and SEM analyses of the 5% (w/v) (type I) and the 15% (w/v) gelatin (type III). For the μ-CT (3D) pictures, the pores are dark gray, and the material is light gray. The scale bars represent 1000 μm (μ-CT) and 500 μm (SEM).

resulting pore size.[14−18] In most studies, the samples were incubated in a freezer for several hours at different temperatures. These studies indicated that the pore size decreased with a decreasing freezing temperature.[14,16,17] Whether the underlying cause of this phenomenon was the actual final freezing temperature, the cooling rate, or a combination of both has never been studied before. The present work demonstrated that the underlying cause is actually the phenomenon of undercooling. In another publication,[15] a complex setup was used to control the cooling rate of a collagen solution. In that study, it was shown that the pore size in collagen matrices decreased with an increasing cooling rate.

Our study aimed to implement a procedure to examine the effect of the cooling rate on the pore size and morphology in gelatin scaffolds. The experimental conditions applied in the

Table 2. Experimental Parameters and Pore Data for Type II and IV Matrixes

sample	type II	type IV
gelatin concentration	10% (w/v)	10% (w/v)
cooling rate	0.15 °C/min	0.83 °C/min
final temperature of freezing	−30 °C	−30 °C
temperature gradient	0	0
porosity (μ-CT)	83 ± 2.63%	84 ± 1.73%
average pore diameter (μ-CT)	135 μm	65 μm
average pore diameter (SEM)	117 ± 37 μm	48 ± 6 μm
porosity (pycnometry)	91 ± 0.7%	89 ± 3%

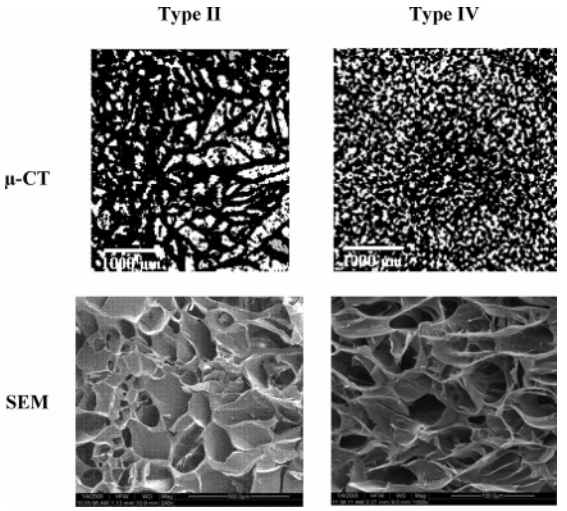

Figure 5. Images of the rapidly cooled gelatin (type IV) and the slowly cooled gelatin (type II), obtained using μ-CT and SEM. The scale bars represent 1000 μm (μ-CT) and 100 and 500 μm (SEM).

present work and the results obtained are summarized in Table 2. For these experiments, a gelatin concentration of 10% (w/v) was selected.

Summarizing the results (Table 2), it can be concluded that a decrease of the cooling rate from 0.83 to 0.15 °C/min resulted in an increase in the average pore diameter from 65 to 135 μm. The difference in median pore size between the rapidly and the slowly cooled gelatin, as analyzed by μ-CT and SEM, is shown in Figure 5. Thus, the slower the cooling rate, the lower the undercooling (difference between the freezing temperature and the actual temperature of the material) and the nucleation rate and the higher the rate of heat and protein transfer. This leads to a lower amount of large pores.[14]

The porosities of both types of hydrogels were identical as shown by μ-CT and He pycnometry. Again, the porosity values, obtained by μ-CT, were lower compared to those obtained by He pycnometry (±80% versus ±90%, respectively).

From Figure 5 (top row), it can also be concluded that the pore interconnectivity was not influenced by the cooling rate. The pores of both types of hydrogels were interconnected, since all pores were labeled in white after performing a 3D analysis. A 3D image of the rapidly cooled gelatin (Figure 6) visualized very clearly a central sample region where the porosity decreased. This corresponded with the zone where the two cooling surfaces (started from the top and bottom of the sample) coincide. A plausible explanation for the observation that the pore diameters in the central region are smaller is decreased heat and protein transfer. Ice crystals are normally formed in the direction of heat transfer.[35] Since the resolution of the μ-CT technique is 10 μm, small pores in the central region were not detected, giving rise to a local decrease in porosity (data not shown).

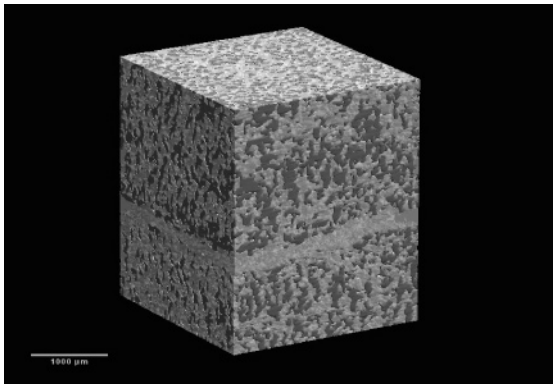

Figure 6. Reconstruction of a section of the rapidly cooled gelatin (type IV), obtained using μ-CT. The pores are dark gray, and the scaffold material is light gray. The scale bar represents 1000 μm.

Table 3. Experimental Parameters and Pore Analysis Data For the Low (Type V) and High (Type VI) Gradient Scaffolds

sample	type V	type VI
gelatin concentration	10% (w/v)	10% (w/v)
cooling rate	0.15 °C/min	0.15 °C/min
final freezing temperature	−30 °C	−30 °C
temperature gradient	10 °C	30 °C
porosity (μ-CT)	76 ± 4.67%	75 ± 3.54%
average pore diameter (μ-CT)		
top	116 μm	330 μm
bottom	20−30 μm	20−30 μm
average pore diameter (SEM)	96 ± 10 μm	283 ± 48 μm
porosity (pycnometry)	92 ± 1.4%	94 ± 0.2%

The 3D reconstruction for the slowly cooled hydrogel type was similar compared to that of the rapidly cooled gelatin, except that no zone was observed where the porosity decreased (data not shown). Probably, the effect of the coinciding cooling surfaces on the pore structure is more pronounced for the rapidly cooled scaffold, since the undercooling is higher in the latter case.

3.4. Effects of Temperature Gradients. With the cryogenic unit, developed in our laboratory (Figure 1), it was also possible to establish a temperature gradient between the top and the bottom of the mold during the freezing step. During the applied temperature gradients, the temperature at the top of the mold was the highest. In the present work, two gradients were applied and compared (10 and 30 °C). The results are summarized in Table 3.

From the data in Table 3 and Figure 7, it can be concluded that the high-temperature gradient (ΔT = 30 °C) resulted in a pore size gradient throughout the scaffold. The pore morphology of the hydrogel is shown in the 3D μ-CT reconstruction and the SEM picture in Figure 7 (top right and bottom right pictures). The pictures clearly indicate the presence of transversal pore channels in the direction of heat transfer.[34] From the data (Table 3), it can be concluded that the pore size decreased from 330 to 20−30 μm when moving through the scaffold from top to bottom. The smallest pores were formed at the side exposed to the lowest temperature (i.e., the bottom of the mold). As discussed in section 3.3, this is related to increased nucleation and reduced heat and protein transfer phenomena.

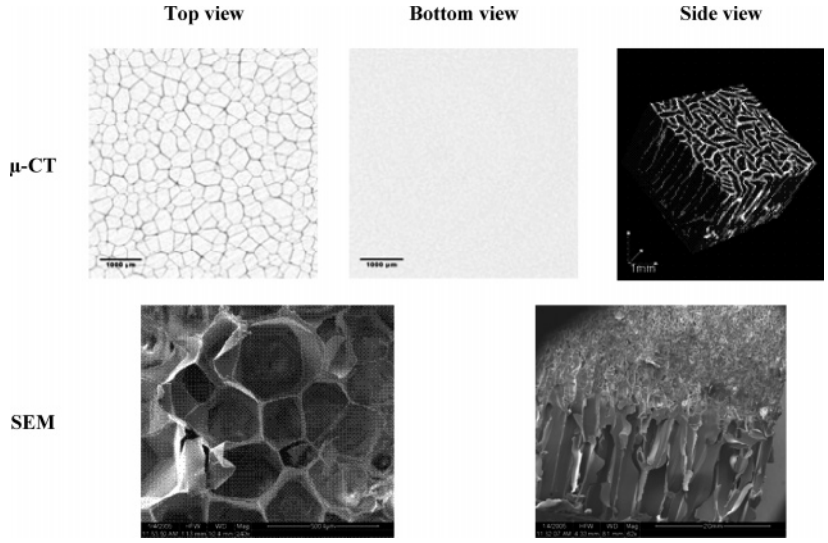

Figure 7. μ-CT and SEM analyses of the top, the bottom, and the side of the scaffold exposed to a temperature gradient of 30 °C (type VI). The scale bars represent 1000 μm (μ-CT) and 500 μm and 2 mm (SEM).

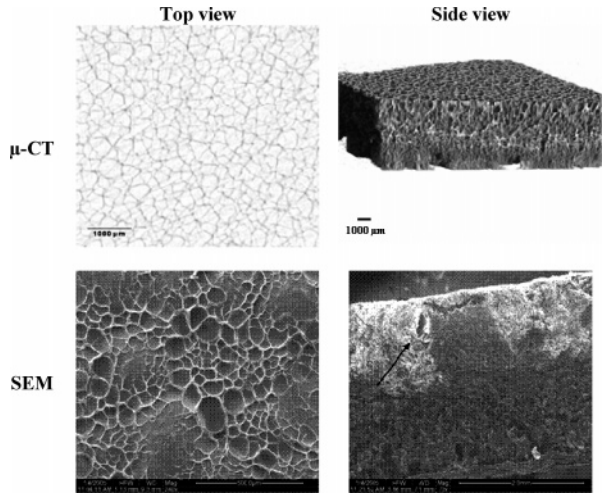

Figure 8. Top views and side views of the low gradient scaffold (type V) obtained using μ-CT and SEM. The scale bars represent 1000 μm (μ-CT) and 500 and 2000 μm (SEM). A crack present in the scaffold is indicated with an arrow.

The applied temperature gradient also resulted in a decrease in porosity, when moving from top to bottom of the scaffold, from 82% to 61%.

When a temperature gradient of 10 °C was applied, the effect on the pore size and the porosity was less pronounced compared to the high-temperature (30 °C) gradient. The pore size decreased from top (116 μm) to bottom (20−30 μm) without altering the porosity. A few cracks were visualized in both the 3D reconstruction and the SEM image (Figure 8, right), which resulted in a local increase of the porosity.

In contrast to the pore size, the porosity of the materials was not affected by the applied temperature gradient. The porosities of both scaffolds, as measured by μ-CT and He pycnometry, were in the range of 75% and 90%, respectively (Table 3). The porosities for both types of hydrogels were similar since the same amount of water was removed through lyophilization.

In our opinion, this is the first paper in which porous gelatin hydrogels were prepared by applying a controlled temperature gradient during the freezing step. This enabled us to develop porous materials containing a pore morphology and pore size that can be fine-tuned by the cryogenic parameters.

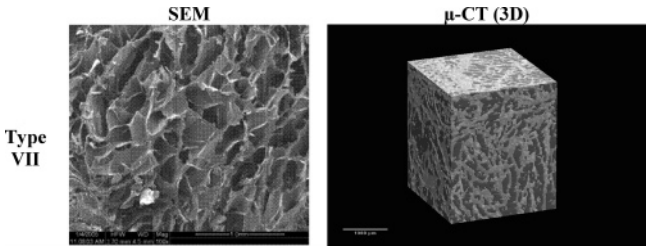

Figure 9. Effect of final freezing temperature on the scaffold structure as visualized by μ-CT and SEM. The structures represent the gelatin scaffold using a final freezing temperature of −10 °C (type VII). The scale bars represent 1000 μm.

Table 4. Experimental Parameters and Pore Data for Type VII and VIII Hydrogels

sample	type VII	type VIII
gelatin concentration	10% (w/v)	10% (w/v)
cooling rate	0.2 °C/min	0.2 °C/min
final temperature of freezing	−10 °C	−30 °C
temperature gradient	0 °C	0 °C
porosity (μ-CT)	85 ± 3.67%	83 ± 2.65%
average pore diameter (μ-CT)	138 μm	147 μm
average pore diameter (SEM)	181 ± 60 μm	182 ± 47 μm
porosity (pycnometer)	92 ± 2%	89 ± 0.9%

3.5. Effect of Final Freezing Temperature. As a last part of the work, we varied the final freezing temperature (−10 vs −30 °C) while keeping the cooling rate constant (0.2 °C/min). The results, as shown in Table 4, indicated that the final freezing temperature did not significantly influence the hydrogel pore size and porosity.

The pores were homogeneously distributed in the scaffold that was treated cryogenically to a final freezing temperature of −10 °C, as shown in Figure 9. Similar results were obtained for the hydrogel that was cooled to −30 °C (data not shown).

The data of the present paper indicate that, of all the parameters varied, the gelatin concentration, the cooling rate, and the applied temperature gradient have the largest effect on the pore size and geometry. The final freezing temperature has a negligible effect.

The gelatin concentration, the cooling rate, and the temperature gradient affect the pore diameter, whereas the pore

geometry and the overall porosity depend mostly on the applied temperature gradient and the gelatin concentration, respectively.

In a forthcoming paper, the in vitro cell interaction properties of the porous gelatin hydrogels developed in the present study will be discussed.

4. Conclusions

The objective of the present work was the development of biodegradable, porous gelatin scaffolds for tissue engineering applications. The porosity was induced by a combination of phase separation and freeze-drying. Three experimental conditions influenced the characteristics of porous gelatin scaffolds: (1) the cooling rate, (2) the polymer concentration, and (3) the implemented temperature gradient. The novel cryo-unit enabled us to produce, in a controlled manner, 3D porous scaffolds in which the pore size, the pore geometry, and the porosity can be easily fine-tuned by variation of the cryogenic parameters. To our knowledge, the development of scaffolds that contain a pore size gradient throughout the material has not been reported previously. The problem of skin formation during cryogenic treatment was solved by applying a soluble layer of un-cross-linked gelatin onto the preformed hydrogel prior to cryogenic treatment. The formed skin can be easily removed by aqueous treatment above the gel−sol transition temperature of gelatin.

The results obtained in the present study will be a valuable tool for research on porous scaffolds, including pore creation techniques as well as nondestructive structure analysis techniques.

Acknowledgment. The authors acknowledge the Institute for the Promotion of Innovation by Science and Technology in Flanders, Belgium, for the Ph.D. funding granted to S. V. and V. C. and the Belgian Research Policy Inter University Attraction Poles (IUAP/PAI-V/03) for financial support. We also thank Olivier Janssens (Department of Solid-State Sciences, Ghent University, Ghent, Belgium) for the SEM measurements and Joris Dierck, Philomain Wauters, and Mario Podevyn (CWFW, Faculty of Sciences, Ghent University, Ghent, Belgium) for designing and building the cryo-unit.

References and Notes

(1) Yannas, I. V. *Proc. Natl. Acad. Sci. U.S.A.* **2000**, *97* (17), 9354−9356.
(2) Tsang, V. L.; Bhatia, S. N. *Adv. Drug Delivery Rev.* **2004**, *56* (11), 1635−1647.
(3) Freyman, T. M.; Yannas, I. V.; Yokoo, R.; Gibson, L. J. *Biomaterials* **2001**, *22* (21), 2883−2891.
(4) Ellis, D. L.; Yannas, I. V. *Biomaterials* **1996**, *17* (3), 291−299.
(5) Zaleskas, J. M.; Kinner, B.; Freyman, T. M.; Yannas, I. V.; Gibson, L. J.; Spector, M. *Biomaterials* **2004**, *25* (7−8), 1299−1308.
(6) Pek, Y. S.; Spector, M.; Yannas, I. V.; Gibson, L. J. *Biomaterials* **2004**, *25* (3), 473−482.
(7) Nehrer, S.; Breinan, H. A.; Ramappa, A.; Young, G.; Shortkroff, S.; Louie, L. K.; Sledge, C. B.; Yannas, I. V.; Spector, M. *Biomaterials* **1997**, *18* (11), 769−776.
(8) Lee, S. B.; Jeon, H. W.; Lee, Y. W.; Lee, Y. M.; Song, K. W.; Park, M. H.; Nam, Y. S.; Ahn, H. C. *Biomaterials* **2003**, *24* (14), 2503−2511.
(9) Kawanishi, M.; Ushida, T.; Kaneko, T.; Niwa, H.; Fukubayashi, T.; Nakamura, K.; Oda, H.; Tanaka, S.; Tateishi, T. *Mater. Sci. Eng., C* **2004**, *24* (3), 431−435.
(10) Chen, G.; Ushida, T.; Tateishi, T. *Mater. Sci. Eng., C* **2001**, *17* (1−2), 63−69.
(11) Whang, K.; Thomas, H.; Healy, K. E.; Nuber, G. *Polymer* **1995**, *36* (4), 837−842.
(12) Mao, J. S.; Zhao, L. G.; Yin, Y. J.; Yao, K. D. *Biomaterials* **2003**, *24* (6), 1067−1074.
(13) Lee, J. E.; Kim, S. E.; Kwon, I. C.; Ahn, H. J.; Cho, H.; Lee, S. H.; Kim, H. J.; Seong, S. C.; Lee, M. C. *Artif. Organs* **2004**, *28* (9), 829−839.
(14) O'Brien, F. J.; Harley, B. A.; Yannas, I. V.; Gibson, L. J. *Biomaterials* **2005**, *26* (4), 433−441.
(15) Schoof, H.; Apel, J.; Heschel, I.; Rau, G. *J. Biomed. Mater. Res.* **2001**, *58* (4), 352−357.
(16) Kang, H. W.; Tabata, Y.; Ikada, Y. *Biomaterials* **1999**, *20* (14), 1339−1344.
(17) Ren, L.; Tsuru, K.; Hayakawa, S.; Osaka A. *J. Non-Cryst. Solids* **2001**, *285* (1−3), 116−122.
(18) Ulubayram, K.; Eroglu, I.; Hasirci, N. *J. Biomater. Appl.* **2002**, *16* (3), 227−241.
(19) Choi, Y. S.; Lee, S. B.; Hong, S. R.; Lee, Y. M.; Song, K. W.; Park, M. H. *J. Mater. Sci.: Mater. Med.* **2001**, *12* (1), 67−73.
(20) Van Den Bulcke, A. I.; Bogdanov, B.; De, Rooze, N.; Schacht, E. H.; Cornelissen, M.; Berghmans, H. *Biomacromolecules* **2000**, *1* (1), 31−38.
(21) O'Brien, F. J.; Harley, B. A.; Yannas, I. V.; Gibson, L. *Biomaterials* **2004**, *25* (6), 1077−1086.
(22) Nam, Y. S.; Park, T. G. *J. Biomed. Mater. Res.* **1999**, *47* (1), 8−17.
(23) Laurencin, C. T.; Ko, F. K.; Attawia, M. A.; Borden, M. D. *Cells Mater.* **1998**, *(8)*, 175−181.
(24) Mooney, D. J.; Baldwin, D. F.; Suh, N. P.; Vacanti, J. P.; Langer, R. *Biomaterials* **1996**, *17* (14), 1417−1422.
(25) Mooney, D. J.; Mazzoni, C. L.; Breuer, C.; McNamara, K.; Hern, D.; Vacanti, J. P.; Langer, R. *Biomaterials* **1996**, *17* (2), 115−124.
(26) Lozinsky, V. I. *Russ. Chem. Rev.* **2002**, *71* (6), 489−511.
(27) Lozinsky, V. I.; Plieva, F. M.; Galaev, I. Y.; Mattiasson, B. *Bioseparation* **2002**, *10* (4−5), 163−188.
(28) Cnudde, V.; Jacobs, P. J. S. In *Proceedings of the International Workshop on X-ray CT for Geomaterials, GeoX2003*, Kumamoto, Japan, Nov 2003; Otani, J., Obara, Y., Eds.; pp 363−371.
(29) Steppe, K.; Cnudde, V.; Girard, C.; Lemeur, R.; Cnudde, J. P.; Jacobs, P. J. S. *J. Struct. Biol.* **2004**, *148* (1), 11−21.
(30) Octopus Home Page. http://ssf.ugent.be/linac/Octopus/.
(31) Dierick, M. *Meas. Sci. Technol.* **2004**, *15* (7), 1366−1370.
(32) Moore, M. J.; Jabbari, E.; Ritman, E. L.; Lu, L.; Currier, B. L.; Windebank, A. J.; Yaszemski, M. J. *J. Biomed. Mater. Res., Part A* **2004**, *71* (2), 258−267.
(33) Jones, A. C.; Milthorpe, B.; Averdunk, H.; Limaye, A.; Senden, T. J.; Sakellariou, A.; Sheppard, A. P.; Sok, R. M.; Knackstedt, M. A.; Brandwood, A.; Rohner, D.; Hutmacher, D. W. *Biomaterials* **2004**, *25* (20), 4947−4954.
(34) Cnudde, V. Ph.D. Thesis Ghent University, Ghent, Belgium, 2005.
(35) Hobbs, P. V. In *Ice Physics*; Clarendon Press: Oxford, U. K., 1974.

BM060684O